JOURNAL OF AGRICULTURAL AND FOOD CHEMISTRY

Article

pubs.acs.org/JAFC

Tissue-Specific Cell Wall Hydration in Sugarcane Stalks

Priscila Maziero,[†,§] Jennifer Jong,[#] Fernanda M. Mendes,[†] Adilson R. Gonçalves,[§] Michaela Eder,[⊥] and Carlos Driemeier*[,†]

[†]Laboratório Nacional de Ciência e Tecnologia do Bioetanol, CTBE/CNPEM, 13083-970 Campinas, São Paulo, Brazil

[§]Departamento de Biotecnologia, EEL-USP, 120602-810 Lorena, São Paulo, Brazil

[#]College of Natural Resources, University of California, Berkeley, California 94720, United States

[⊥]Department of Biomaterials, Max-Planck-Institute of Colloids and Interfaces, Wissenschaftspark Golm, Am Muhlenberg 1, 14476 Potsdam, Germany

Supporting Information

ABSTRACT: Plant cell walls contain water, especially under biological and wet processing conditions. The present work characterizes this water in tissues of sugarcane stalks. Environmental scanning electron microscopy shows tissue deformation upon drying. Dynamic vapor sorption determines the equilibrium and kinetics of moisture uptake. Thermoporometry by differential scanning calorimetry quantifies water in nanoscale pores. Results show that cell walls from top internodes of stalks are more deformable, slightly more sorptive to moisture, and substantially more porous. These differences of top internode are attributed to less lignified walls, which is confirmed by lower infrared spectral signal from aromatics. Furthermore, cell wall nanoscale porosity, an architectural and not directly compositional characteristic, is shown to be tissue-specific. Nanoscale porosities are ranked as follows: pith parenchyma > pith vascular bundles > rind. This ranking coincides with wall reactivity and digestibility in grasses, suggesting that nanoscale porosity is a major determinant of wall recalcitrance.

KEYWORDS: *accessibility, recalcitrance, grass, bagasse, lignocellulose*

INTRODUCTION

The lignocellulosic biomass of plant cell walls is a vastly underexploited renewable resource. It has the potential to replace a significant share of fossil carbon that is presently converted into materials, chemicals, and liquid fuels. If properly prepared, it may also serve as animal forage. Especially promising are lignocelluloses from grasses, which include agricultural residues from major staple crops (e.g., maize, wheat, rice) as well as candidate cultures tailored for biomass and bioenergy production (e.g., miscanthus, switchgrass). Sugarcane is a prominent source of grass biomass because it is a well-established crop already deployed in large scale and processed in centralized units, coproducing sugar, bioelectricity, and ethanol.[1,2] Furthermore, the productivities of some tailored bioenergy cultures (not yet deployed in large scale) are similar to those presently achieved with sugarcane.[3] Current practice is to harvest the sugarcane stalks, crush the stalks to extract the sucrose-rich juice, and combust the lignocellulosic residue (the bagasse) for heat and power. Conversion of bagasse into more valuable products is presently under intense investigation.[1,2]

The stalks of sugarcane, a monocotyledonous plant,[4,5] are similar to those of many other grasses. The stalk consists of series of nodes, the attachment points for leaves, and internodes. A cross section of an internode shows numerous vascular bundles embedded in ground tissue (parenchymatous cells) (Supporting Information Figure S1). The vascular bundles are more densely distributed toward the hypo- and epidermis, the outermost layers of the stalk. In grasses, cell wall reactivity (in wet chemical processing) and digestibility (by cellulolytic enzymes or rumen microorganisms) are known to depend both on tissues and on cell development stage.[6−12] Mature as well as peripheral tissues are more recalcitrant; younger as well as more internal (central) tissues are less so. This has been primarily attributed, with partial success, to differences in wall composition, with emphasis on the contents of lignin and aromatics of lower molecular weight.[6,8,10]

Adding to recent compositional[8,13−15] and structural[16] studies to better understand sugarcane biomass, the present paper investigates the water that hydrates the cell walls of sugarcane stalks. This water is intentionally omitted by compositional analyses, although water is consistently present, especially under biological and wet processing conditions. Moreover, although hydration is certainly correlated to dry composition (e.g., hydrophilic polysaccharides versus hydrophobic aromatics), hydration is further influenced by wall supramolecular architecture, to which compositional analysis is blind. Water, besides being a reactant (e.g., in hydrolysis), is the medium of nanometric pathways through which reactants and enzymes can penetrate the walls, and low-molecular-weight reaction products can leave the walls.

The present study analyzes cell wall hydration by combining three analytical techniques: environmental scanning electron microscopy (ESEM), which can provide high-magnification images in natural wet states; dynamic vapor sorption (DVS), which is primarily sensitive to the first hydration layers

Received: March 20, 2013
Revised: May 27, 2013
Accepted: May 28, 2013
Published: June 5, 2013

contacting the solid; and thermoporometry by differential scanning calorimetry (TP-DSC), which probes wall nanoscale porosity in wet state. Because observed hydration (especially nanoscale porosity) is ranked coincidentally to cell wall reactivity and digestibility, our results bring an architectural (not directly compositional) explanation for tissue-specific recalcitrance.

MATERIALS AND METHODS

Sugarcane for ESEM. Samples imaged by ESEM were dissected from a sugarcane stalk collected at Usina da Pedra, Serrana, São Paulo, Brazil, in September 2011 (during cane harvest season). This cane had been growing for about 12 months. Four centimeter long segments were separated from internodes located in the bottom, middle, and top parts of the plant. The entire segments were extracted with distilled water in a Soxhlet apparatus with nine cycles of 8 h, as described elsewhere.[17] This procedure is expected to remove nonstructural sugars, mainly sucrose residues, generating extracted materials similar to sugarcane bagasse (the sucrose-extracted lignocellulosic residue from cane mills). For ESEM imaging, 600 μm thin cross sections were prepared with a rotary microtome (Leica RM2255) and immediately stored in distilled water.

Sugarcane for DVS and TP-DSC. Samples for quantitative inferences by DVS and TP-DSC were dissected from five sugarcane stalks (biological replicates, variety SP80-3280) collected at Fazenda Vitória, Piracicaba, São Paulo, Brazil, in June 2012 (during cane harvest season). The canes had been growing for about 9 months. Internodes were separated from the bottom, middle, and top parts of the stalks (tentatively the bottom-most, exact middle, and topmost internodes, but this identification is sometimes imprecise). Tissues were separated from the entire internodes, except for regions within ≈5 mm of nodes and free edges exposed during storage.

The outer peripheral layer (≈5 mm) with a high density of vascular bundles was separated. Wax and epidermis were removed by peeling until the light green tissue underneath showed. In addition, inner tissues were isolated and separated into *vascular bundles* and *parenchyma* by gently pulling the bundles between tweezers and fingertips. The separated tissues (see Figure S2 in the Supporting Information) were stored at 5 °C immersed in a mixture of ethanol and water (20:80, v/v). Measured properties showed no significant dependence with storage times (maximum of 30 days), indicating that the storage conditions did not significantly modify the cell walls. Following the usual nomenclature in sugarcane biomass studies, the peripheral 5 mm layer was named *rind*, whereas the inner region was named *pith*.

Sample preparation for DVS and TP-DSC analysis must include the careful removal of water-soluble compounds (that promote spurious shifts in measured water phase transitions) while keeping the cell walls wet and as undamaged as possible. Hence, the wet (never-dried) samples (of 5−20 mg dry matter) were cut into millimetric pieces with a scalpel, fragmenting tissues and opening cells (i.e., exposing intracellular media). The cut tissues were rinsed with water to remove soluble compounds. Further removal of soluble compounds was achieved by leaving the solids immersed in 50 mL of distilled water for 24 h, a procedure done twice. This dilution procedure was verified to be sufficient for the performed analyses, because additional dilution cycles promoted no significant change to measured properties.

Bagasse for TP-DSC. Sugarcane bagasse was collected from the bagasse pile of Usina da Pedra, Serrana, São Paulo, Brazil, in November 2011. After collection, the bagasse was air-dried to 8−10% equilibrium moisture content. A representative mass was sieved by a column (Analysette 3 PRO system, Fritsch GmbH) with two sieves, resulting in three fractions: retained at the (i) first sieve (1.18 mm mesh), (ii) second sieve (0.15 mm mesh), and (iii) bottom of the column (passed both sieves). These fractions (see Figure S3 in the Supporting Information) were respectively named coarse, intermediate, and fine. Before DVS and TP-DSC analyses, bagasse fractions were cut into millimetric pieces with a scalpel, followed by washing and dilution of soluble compounds as performed for tissues dissected from sugarcane stalks (see description under Sugarcane for DVS and TP-DSC).

Environmental Scanning Electron Microscopy. ESEM is a powerful tool in biomaterials research because specimens can be imaged at high magnifications in natural wet states and without a conductive surface. The main difference from conventional scanning electron microscopy is the presence of a small amount of gas in the specimen chamber. If the gas is water vapor and the sample is cooled, it is possible to image wet specimens. Furthermore, ionization processes in the sample chamber allow imaging of insulator specimens without conductive coatings.[18−20]

Imaging was performed in an FEI FE-ESEM Quanta 600 with an accelerating voltage of 12 kV and a gaseous secondary electron detector. The 600 μm thin never-dried cross sections were placed on top of the cooling stage immersed in water. The temperature was set at 7 °C and the chamber pressure kept above 8 Torr during evacuation of the sample chamber, which prevents the sample from drying. After evacuation, the chamber pressure was reduced stepwise to allow evaporation of water from the sample surface. Care was taken to prevent the sample from any drying. Images of the fully hydrated samples were taken when the surface covering water film disappeared. Subsequent drying of the samples was performed by further decreasing the chamber pressure to 1.5−0.75 Torr. After reaching equilibrium conditions (no further drying), micrographs were taken.

Dynamic Vapor Sorption. DVS provides information about the equilibrium and the kinetics of water desorption and sorption. Equilibrium analysis is done with desorption and sorption isotherms, in which water contents are measured as a function of relative humidity (RH).[21,22] Kinetic analysis is based on characteristic times that are inferred from the transient water content induced by a change in RH.[23−25]

DVS analysis was performed with a Q5000 SA instrument (TA Instruments, USA) with metalized quartz pans.[25] Wet samples (of ≈1 mg dry mass) were prepared by homogenizing materials dissected from the five sugarcane stalks as described under Sugarcane for DVS and TP-DSC. DVS analysis initially equilibrated samples at 50 °C and 95% RH, followed by stepwise RH decrement for water desorption until the sample was completely dried and then stepwise RH increment for water sorption. Sample mass was monitored continuously. Each RH step took 60 min except at 0% RH, which lasted 180 min to improve definition of sample dry mass. Sorption isotherms were built from water contents (per unit of dry mass) at the end of each RH step. Isotherms up to 80% RH were analyzed by the Hailwood−Horrobin (HH) model,[21] which describes isotherms from three coefficients: (i) mass of monolayer hydration (ML H_2O); (ii) equilibrium constant of monolayer hydration; and (iii) equilibrium constant of the so-called dissolved water. For the present work, only ML H_2O from sorption is reported because ML H_2O from desorption is likely biased by water pockets remaining from water-swollen states.[25] ML H_2O (given in units of water mass per sample dry mass) estimates the amount of water in molecular contact with the matrix.

Thermoporometry. Thermoporometry (also named cryoporometry) measures solid−liquid phase transitions that are shifted in temperature because they undergo nanoscale confinement.[26,27] Thermoporometry is well suited to lignocellulosic materials because nanoscale porosity is measured in wet samples. TP-DSC discriminates three types of water: (i) free water; (ii) nonfreezing bound water (NFW); and (iii) freezing bound water (FBW). Free water is water not bound to cell walls, including water excess added during sample preparation (not an intrinsic material property); free water is measured from ice melting at 0 °C. NFW is water closely associated with solid surfaces; it is calculated (although with high uncertainty)[25] as the difference between total sample water and total freezing water. FBW is the major result from TP-DSC. FBW is water confined by the solid in a way that shifts ice−water phase transitions; it is measured from ice melting *below* 0 °C. Because the estimated pore diameters associated with FBW are of the order of *nanometers*, FBW is primarily attributed to be confined inside the cell walls, not in the much larger *micrometric* volumes of cell lumina and intercellular pits.

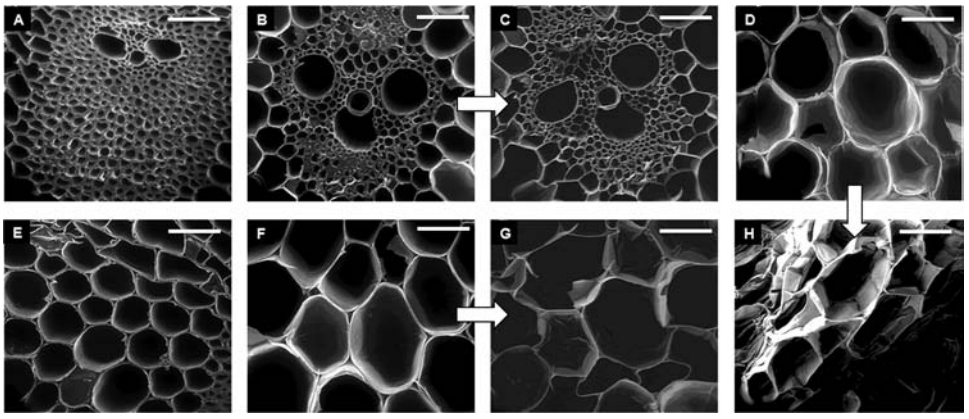

Figure 1. Environmental scanning electron microscopy images from sections of sugarcane stalks: vascular bundles from (A) bottom rind in wet state and bottom pith in (B) wet and (C) dry states; parenchyma from (D) top pith in wet state, (E) bottom rind in wet state, bottom pith in (F) wet and (G) dry states, and (H) top pith in dry state. Chamber pressures for dry states are either 0.75 Torr (C, G) or 1.5 Torr (H). Scale bars are 100 μm. Arrows point from wet to dry images acquired in the same specimen region.

TP-DSC was performed using a Q200 instrument with an RCS90 cooling unit (TA Instruments).[25] Samples (0.5−3.6 mg dry mass) saturated with deionized water were inserted in Tzero aluminum pans, which were then sealed with hermetic lids. TP-DSC analysis was done by freezing the samples to −70 °C followed by stepwise increase of temperature to melt the formed ice. Heat from ice melting was calorimetrically detected and converted to ice mass. Ice that melted below 0 °C was associated with FBW confined in pores. Pore diameters ⌀ were calculated from melting temperature depression (ΔT) using the Gibbs−Thomson relation $⌀ = -2K_c/\Delta T$, with K_c = 19.8 nm K.[25] The result of each measurement was the cumulative FBW (in units of ice mass per sample dry mass) as a function of pore diameter ⌀.

Fourier Transform Infrared Spectroscopy (FTIR). FTIR was performed in attenuated total reflection (ATR) mode using a Spectrum 400 spectrophotometer with a Universal ATR accessory and ZnSe crystal (Perkin-Elmer, USA). Spectra were acquired in the 650−4000 cm^{-1} range, averaging 32 scans with 4 cm^{-1} resolution. Spectral baselines were subtracted. Tissues described under Sugarcane for DVS and TP-DSC were analyzed, with materials from the five sugarcane stalks mixed and homogenized. Parenchyma samples did not require additional preparation, whereas vascular bundles and rind were powdered in a ball-mill Geno/Grinder. Mild milling conditions were chosen to promote minimum cellulose amorphization. All samples were air-dried for FTIR analysis.

RESULTS AND DISCUSSION

Wet and Dry Tissue Visualization. Xylem and phloem of the vascular bundles are surrounded by sclerenchymatous fibers (Figure 1A−C). In a typical vascular bundle from the rind region (Figure 1A), xylem and phloem are smaller and the sheath of the sclerenchyma fibers is much more prominent than that from the pith region (Figure 1B). In Figure 1C the vascular bundle (B) is shown in the dried state: cell wall shrinkage due to water loss leads to tissue deformation of the whole vascular bundle. Wet and dry vascular bundles of the bottom and top rind of the stalk are depicted in Figure S4 in the Supporting Information. Due to the higher cell wall proportion in rind vascular bundles, their deformation seems to be more pronounced.

Compared to fibers in vascular bundles, parenchyma cells (Figure 1D−H) have thinner cell walls and larger diameters, which are even larger in pith (Figure 1D,F−H) than in rind (Figure 1E). Parenchyma cells substantially deform upon drying. This is exemplified by parenchyma cells from pith of the bottom (Figure 1F,G) and top (Figure 1D,H) of the stalk. Parenchyma is more susceptible to deformation because of their thin cell walls coupled to large cell diameters. Furthermore, panels D and H of Figure 1 exemplify that parenchyma from the top deforms more, a result that was repeatedly observed. Cells from the top internode are younger, and their enhanced fragility can be attributed to less lignified walls, which is supported by the results presented henceforth.

Monolayer Hydration. Figure S5 in the Supporting Information presents the raw data of a DVS analysis, with RH and sample mass as a function of time. Sample masses at the end of RH steps are analyzed through sorption isotherms like those of Figure 2. Analysis of isotherms employing the HH

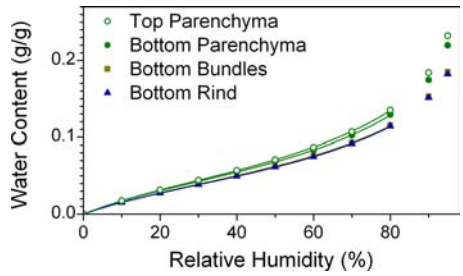

Figure 2. Vapor sorption isotherms for selected sugarcane fractions dissected from the stalks. Symbols are measured water contents (at the end of each relative humidity step), and lines are fits with the Hailwood−Horrobin model (up to 80% relative humidity). Other cane fractions are not shown to avoid further overlapping of data points.

model leads to the ML H_2O coefficients reported in Table 1. Precisions (1σ) in ML H_2O are of about 0.0015 g/g, as estimated from replicate analyses of selected samples. Differences in sorption isotherms (Figure 2) and ML H_2O derived from them (Table 1) are small and, in several cases, not significant. Water contents in Figure 2 are well correlated to ML H_2O reported in Table 1, and Figure 2 omits some samples to avoid the presentation of severely overlapped isotherms.

DVS primarily probes the first few hydration layers surrounding wall structural polysaccharides, which are hydrophilic. Thus, features relevant for DVS analysis include cellulose association with hemicelluloses, cellulose crystallite width,[28] and cellulose crystallinity. (A recent study[29] indicated minimum noncrystalline cellulose.) As will be later discussed aided by TP-DSC and FTIR results, the existing differences in ML H_2O can

Table 1. Selected Parameters from the Sugarcane Fractions Dissected from the Stalks[a]

cane fraction	ML H_2O (g/g)	FBW < 400 nm (g/g)	FTIR at 1515 cm^{-1}
bottom parenchyma	0.056	0.37	0.047
middle parenchyma	0.054	0.24	0.063
top parenchyma	0.060	0.47	0.044
bottom bundles	0.055	0.18	0.062
middle bundles	0.053	0.18	0.062
top bundles	0.053	0.23	0.047
bottom rind	0.052	0.13	0.060
middle rind	0.053	0.14	0.048
top rind	0.056	0.33	0.030

[a]The parameters are monolayer hydration from Hailwood−Horrobin analysis of sorption isotherms (ML H_2O), freezing bound water cumulated up to pores of 400 nm (FBW < 400 nm), and normalized absorbance of Fourier transform infrared spectra at 1515 cm^{-1}

be primarily attributed to variable aromatic contents. Hence, the small (<15%) differences in ML H_2O (Table 1) support little tissue-specific supramolecular arrangement of cell wall polysaccharides.

Desorption and Sorption Characteristic Times. Figure S5 in the Supporting Information evidences that the kinetics of desorption and sorption present a fast and a slow component during each RH step. This behavior has been observed and discussed in previous works.[23−25] The fast component depends on sample mass and is likely limited by mass or heat transport.[25] Hence, the fast component is not an intrinsic material property and will not be addressed here. Following ref 25 the slow component is represented by $t_{1/16} - t_{1/8}$, where $t_{1/16}$ and $t_{1/8}$ are the times required to reach, respectively, $^{15}/_{16}$ and $^{7}/_{8}$ of the mass change within each RH step.

Figure 3 shows that all of the slow characteristic times of desorption are around $t_{1/16} - t_{1/8} \approx 14$ min. Taking RH across

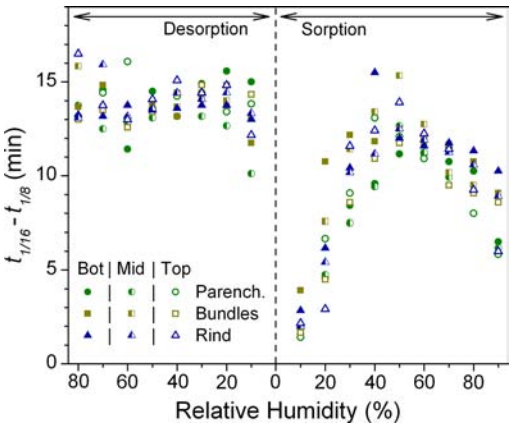

Figure 3. Slow characteristic times ($t_{1/16} - t_{1/8}$) of dynamic vapor sorption for the sugarcane fractions dissected from the stalks.

the 10−80% interval, the mean and standard deviation of desorption characteristic times were calculated for each dissected fraction. Means are within 12.6−14.2 min, and standard deviations are below 1.3 min. This is strikingly close to what had been observed by applying the same method to a wide spectrum of celluloses isolated from plants (means within 12.8−13.8 min, standard deviations within 1−2 min).[25] Because results from cane (Figure 3) are very similar to those from isolated celluloses,[25] the present study provides additional support to the previous observation that *desorption* kinetics is primarily independent of the structure of the (ligno)cellulosic solid. The general desorption kinetics may be due to evaporation from the aforementioned water pockets remaining from water-swollen states.[25]

Sorption characteristic times, on the other hand, were appreciably variable across the wide spectrum of celluloses isolated from plants,[25] indicating a role of the variable cellulose structure. The sorption characteristic times from the isolated celluloses with the highest monolayer hydrations[25] are similar to those observed for the fractions dissected from cane (Figure 3). By comparison among the cane fractions of Figure 3, no consistent differences are observed (note that, for each RH, vertical dispersion of data points from sorption characteristic times is comparable to those from desorption). Hence, the characteristic times of sorption also support little difference in the supramolecular arrangement of the hydrophilic cell wall polysaccharides, considering the few hydration layers probed by DVS. The causes for the dependence of sorption characteristic time on RH are presently unknown. An underlying phenomenon may be the viscoelastic relaxation of the lignocellulosic matrices.[24]

Nanoscale Porosity. Several research groups have been applying thermoporometry to processed lignocellulosic materials,[25,30−34] but similar efforts have not been dedicated to raw plant tissues. Figure S6 in the Supporting Information shows a raw TP-DSC thermogram, with temperature and heat flow as a function of time. It is worth explaining here why the present as well as previous studies[25,31−34] have performed TP-DSC of cellulosic solids by *stepwise melting* protocols. *Melting* is preferred to freezing because freezing temperatures are biased by water supercooling, and *stepwise* is preferred to continuous because the isothermal intervals accurately define the heat flow baseline, which is critical to accurately resolve the ice melting signals that are spread from −60 to 0 °C.

Ice melting below 0 °C is considered FBW that is given as a function of pore diameter ⌀ calculated from melting temperature (see Thermoporometry). Figure 4 presents analyzed results of TP-DSC obtained from the sugarcane fractions separated by dissecting the stalks (described under Sugarcane for DVS and TP-DSC) as well as by sieving the bagasse (described under Bagasse for TP-DSC). All of the FBW curves of Figure 4 rise monotonically, as expected for cumulative distributions. In addition, all of the FBW curves have similar shape, although they vary in height. The similar shape suggests that FBW of all samples is determined by common features of cell wall architecture, likely associated with the geometry of the tridimensional network of cellulose microfibrils. The variable heights of FBW curves, however, indicate that the amount of water in nanometric pores is a tissue-specific property. Henceforth, the cumulative FBW is termed *cell wall porosity*, to be understood as an average characteristic of the analyzed masses.

TP-DSC analysis of the sugarcane fractions dissected from the stalks (Figure 4 top) reveals that cell walls from the top of the stalks are more porous. This enhanced porosity is observed for parenchyma, vascular bundles, and, most pronouncedly, for cell wall material from the rind. Comparison between bottom and middle fractions of the stalk evidences no porosity

dx.doi.org/10.1021/jf401243c | J. Agric. Food Chem. 2013, 61, 5841−5847

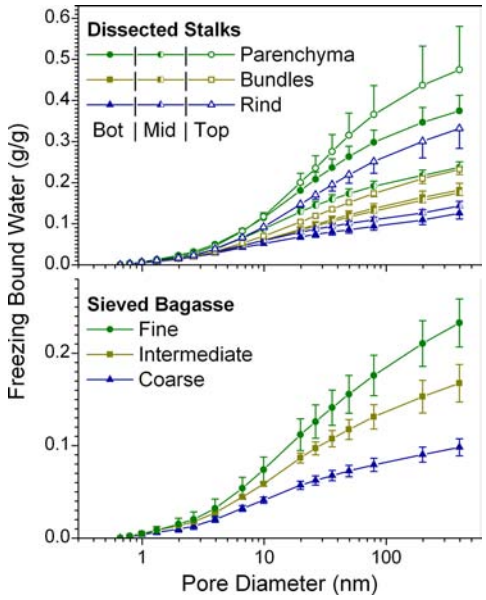

Figure 4. Analyzed thermoporometry data for the sugarcane fractions separated either by dissecting the stalks (top) or by sieving the bagasse (bottom). Data points are means, and error bars are standard deviations of the means calculated from five biological replicates (dissected stalks) or four independent samples (sieved bagasse). For better visualization the top graph omits halves of the symmetric error bars.

differences for vascular bundles and rind, whereas parenchyma from the bottom is more porous than that from the middle. It is noteworthy that a 4-fold difference exists between maximum (top parenchyma) and minimum (bottom rind) cell wall porosities. This is a dramatic difference compared to the maximum difference of ≈15% observed in ML H_2O determined by DVS (see Table 1). Furthermore, neglecting the top of the stalks (which can be considered exceptional), cell wall porosities are ranked as follows: pith parenchyma > pith vascular bundles > rind.

Bagasse is a mixture of tissues from sugarcane stalks that have been crushed in sugar mills. Sizes and shapes of bagasse particles do not discriminate whether they originate from the bottom, middle, or top of the stalk. Nevertheless, the coarser bagasse particles originate primarily from the rind and the fines, primarily from pith parenchyma. The intermediate fraction has mixed origin, with significant contributions from rind and pith, vascular bundles, and parenchyma. Because of the industrial potential of bagasse, it is important to verify whether differences in cell wall porosity are observable in bagasse as well. Results of Figure 4 (bottom graph) evidence that indeed cell wall porosities differ. Porosities of sieved bagasse fractions are ranked as follows: fine > intermediate > coarse. This is consistent with the ranking (parenchyma > vascular bundles > rind) derived from tissues dissected from the crude stalks. Moreover, because tissue separation is less effective in sieved bagasse, the magnitudes of porosities are similar between bagasse and dissected stalks. This similarity indicates that cell wall porosity is not substantially altered by the industrial crushing of sugarcane for extraction of its sucrose.

Aromatic Contents. ML H_2O and FBW (see Table 1) are mass ratios (water mass/dry mass). Differences in these ratios may originate from the water mass (numerator) as well as from the dry mass (denominator). The presence of aromatics, lignin, and phenolic acids of lower molecular weight[8,9] may change these ratios. Because of their predominant hydrophobic character, aromatics contribute little to water monolayer sorption (the numerator of ML H_2O), but they still contribute entirely to the dry mass (the associated denominator). Hence, due to a denominator effect, aromatic compounds tend to decrease ML H_2O approximately in proportion to the aromatic content in the sample. On the other hand, wall lignification is thought to take place primarily by filling of pre-existing pores in the polysaccharide network.[35] In this case aromatic compounds decrease FBW by reducing the porosity itself (the numerator of FBW) *and* by increasing the dry mass (the associated denominator). Because the numerator follows aromatic content in absolute and not relative terms, the effect of the numerator tends to dominate FBW changes. For instance, if one assumes (for simplicity) aromatic compounds have the same density as ice, then adding x mg of pore-filling lignin promotes an *absolute* loss of x mg of freezing bound water measured by TP-DSC.

Considering these expected roles of aromatics, it was verified whether the aromatic contents vary among the sugarcane fractions dissected from the stalks. Figure 5 compares FTIR

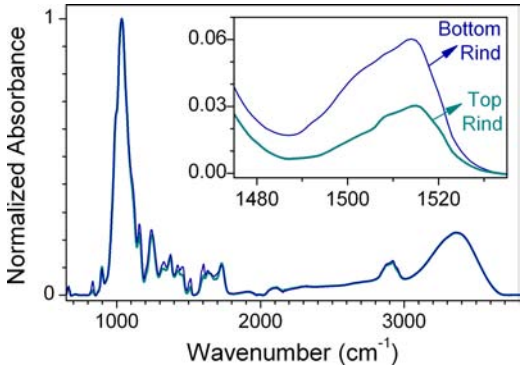

Figure 5. Fourier transform infrared spectra of bottom and top rind fractions dissected from sugarcane stalks. Absorbance is shown normalized by its level at 1035 cm^{-1}, corresponding to the maximum of overlapped alcohol bands originated mainly from carbohydrates. (Inset) Band of aromatic skeletal vibration near 1515 cm^{-1}, evidencing lower aromatic content in the top rind fraction.

spectra from the bottom and top rinds. Spectra were normalized by absorbance at 1035 cm^{-1}, corresponding to the region of maximum absorbance, which is associated with alcohol (C−OH) bands[36] from polysaccharides. Spectra of bottom and top rind overlap in most spectral regions, but differ appreciably in the 1515 cm^{-1} region of aromatic skeletal vibrations,[37,38] as shown in the inset of Figure 5. The difference evidences lower aromatic content in the top rind compared to the bottom rind. Appreciable differences in other spectral bands (835, 1325, 1425, 1460, and 1605 cm^{-1}) may also be attributed to the difference in aromatic contents.[37] As expected from the discussion of the previous paragraph, the lower aromatic content in the top rind is associated with *slightly* higher ML H_2O and *substantially* higher FBW (see Table 1 and Figure 4).

To further investigate the role of aromatics, Figure 6 presents ML H_2O and FBW as a function of normalized absorbance at 1515 cm^{-1}. The same data (but lacking the error bars) are presented in Table 1. The trends are similar for ML H_2O and FBW, but for FBW the differences are more significant and have much higher magnitudes. Within a given tissue (parenchyma, bundles, or rind) there are negative correlations

dx.doi.org/10.1021/jf401243c | J. Agric. Food Chem. 2013, 61, 5841−5847

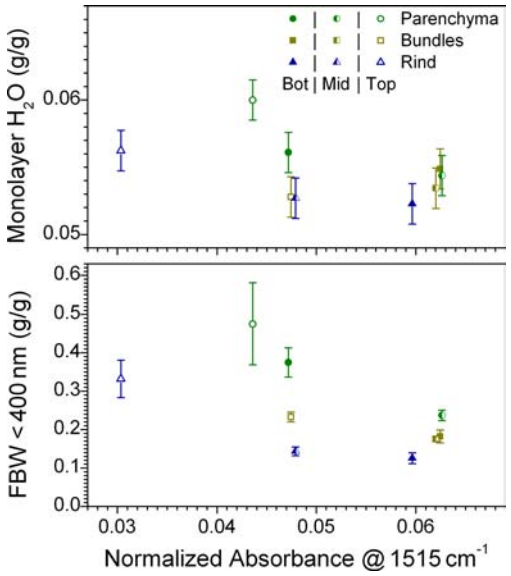

Figure 6. Cell wall hydration compared to infrared signal from aromatics. Monolayer hydration (from vapor sorption, top graph) and freezing bound water (FBW) cumulated up to 400 nm pore diameter (from thermoporometry, bottom graph) are shown against normalized infrared absorbance at 1515 cm^{-1}. Data points for FBW are means of five biological replicates, whereas for monolayer H_2O and infrared absorbance data points are single measurements made with the five replicates homogenized into a single sample. Error bars estimate 1σ precision, either inferred from replicate analysis of selected samples (top graph) or calculated as the standard deviation of the mean from the five biological replicates (bottom graph).

between FBW and 1515 cm^{-1} absorbance. These negative correlations are consistent with aromatics filling wall pores that would otherwise contribute to FBW. In particular, the appreciable porosity of top rind can be attributed to its much lower aromatic content. Along this line, the aromatic signal of bottom parenchyma is lower than that of middle parenchyma, explaining the associated difference in wall porosity, although it remains unclear why bottom parenchyma has lower aromatic content. Furthermore, the trends reveal that, for a given 1515 cm^{-1} absorbance, FBW is higher for parenchyma, intermediate for vascular bundles, and lower for rind. This indicates that FBW cannot be explained only by aromatic content. Because wall porosity also depends on its nanoscale architecture, the trend indicates appreciable architectural differences among the tissues.

Other Tissue-Specific Properties. Tissue-specific cell wall porosity revealed in the present work adds to other known structural differences between tissues. Particle porosity, which is primarily determined by the volume ratio occupied by cell lumina, is higher in parenchyma compared to fibrous bagasse particles.[39,40] Parenchyma walls are also thinner,[41] which is associated with higher specific surface areas as measured (in dry samples) by N_2 sorption.[40] Another purely architectural characteristic is the microfibril angle, which is presumably related to porosity because nanoscale pores are defined by the geometry of the microfibril network. In sugarcane vascular bundles the mode of microfibril angle distributions was found between 10.6° and 40.0°, decreasing, on average, from the central part of pith (32.4°) to rind (25.0°).[16]

Wall Porosity and Degradability. Cell wall porosity is critical for molecular access and transport through the walls. Accessibility[42−45] is especially critical for the activity of lignocellulose degrading enzymes (of ≈5 nm size) working in the digestive tract of some animals (e.g., ruminants) as well as in industrial plants for lignocellulose conversion. The ranking of wall digestibility[6−12] coincides with the ranking of wall porosity: younger as well as more internal (from pith) walls are more digestible and porous, mature as well as peripheral (from rind) walls are less so. This common ranking coupled to the critical role attributed to enzyme accessibility suggests that the reported tissue-specific wall porosity is a main cause of tissue-specific degradability.

■ ASSOCIATED CONTENT

Supporting Information

Figures S1−S6. This material is available free of charge via the Internet at http://pubs.acs.org.

■ AUTHOR INFORMATION

Corresponding Author

*(C.D.) E-mail: carlos.driemeier@bioetanol.org.br. Phone: +55 19 3518 3180. Fax: +55 19 3518 3164.

Funding

Research supported by CNPq and FAPESP (Grants 2009/00874-5 and 2010/05523-3). Cal Energy Corps is acknowledged for J.J.'s internship in CTBE/CNPEM.

Notes

The authors declare no competing financial interest.

■ ACKNOWLEDGMENTS

We thank Adriana Grandis for kind provision of sugarcane stalks, Karen Marabezi for FTIR analysis, and Susan Weichold for supporting ESEM operation.

■ REFERENCES

(1) Cortez, L. A. B., Ed. *Sugarcane Bioethanol − R&D for Productivity and Sustainability*; Blucher: São Paulo, Brazil, 2010.

(2) Soccol, C. R.; Vandenberghe, L. P. D. S.; Medeiros, A. B. P.; Karp, S. G.; Buckeridge, M.; Ramos, L. P.; Pitarelo, A. P.; Ferreira-Leitão, V.; Gottschalk, L. M. F.; Ferrara, M. A.; da Silva Bon, E. P.; de Moraes, L. M. P.; Araújo, J. D. A.; Torres, F. A. G. Bioethanol from lignocelluloses: status and perspectives in Brazil. *Bioresour. Technol.* **2010**, *101*, 4820−4825.

(3) Somerville, C.; Youngs, H.; Taylor, C.; Davis, S. C.; Long, S. P. Feedstocks for lignocellulosic biofuels. *Science* **2010**, *329*, 790−792.

(4) Van Dillewijn, C. El tallo. In *Botánica de la Caña de Azúcar*; Instituto del Libro: La Habana, Cuba, 1951; pp 1−29.

(5) Moore, H. P. Anatomy and morphology in sugarcane improvement through breeding. In *Sugarcane Improvement through Breeding*; Heinz, D. J., Ed.; Elsevier: Amsterdam, The Netherlands, 1987; pp85−142.

(6) Jung, H. G.; Casler, M. D. Maize stem tissues: impact of development on cell wall degradability. *Crop Sci.* **2006**, *46*, 1801−1809.

(7) Zeng, M.; Ximenes, E.; Ladisch, M. R.; Mosier, N. S.; Vermerris, W.; Huang, C.-P.; Sherman, D. M. Tissue-specific biomass recalcitrance in corn stover pretreated with liquid hot-water: enzymatic hydrolysis (part 1). *Biotechnol. Bioeng.* **2012**, *109*, 390−397.

(8) Siqueira, G.; Milagres, A. M. F.; Carvalho, W.; Koch, G.; Ferraz, A. Topochemical distribution of lignin and hydroxycinnamic acids in sugar-cane cell walls and its correlation with the enzymatic hydrolysis of polysaccharides. *Biotechnol. Biofuels* **2011**, *4*, 7.

(9) Anderson, W. F.; Akin, D. E. Structural and chemical properties of grass lignocellulose related to conversion for biofuels. *J. Ind. Microbiol. Biotechnol.* **2008**, *35*, 355−366.

(10) Akin, D. E. Plant cell wall aromatics: influence on degradation of biomass. *Biofuels, Bioprod. Biorefin.* **2008**, *2*, 288−303.

(11) Akin, D. E. Histological and physical factors affecting the digestibility of forages. *Agron. J.* **1989**, *8*, 117−125.
(12) Costa, T. H. F. *Evaluation of Recalcitrance at Different Internode Regions Derived from Hybrid Sugarcane with Varying Amounts of Lignin*. Master's dissertation, Engineering School of Lorena, Oct 2012.
(13) Peng, F.; Ren, J.-L.; Xu, F.; Bian, J.; Peng, P.; Sun, R.-C. Comparative study of hemicelluloses obtained by graded ethanol precipitation from sugarcane bagasse. *J. Agric. Food Chem.* **2009**, *57*, 6305−6317.
(14) Peng, F.; Ren, J.-L.; Xu, F.; Bian, J.; Peng, P.; Sun, R.-C. Fractional study of alkali-soluble hemicelluloses obtained by graded ethanol precipitation from sugar cane bagasse. *J. Agric. Food Chem.* **2010**, *58*, 1768−1776.
(15) Souza, A. P.; Leite, D. C. C.; Pattathil, S.; Hahn, M. G.; Buckeridge, M. S. Composition and structure of sugarcane cell wall polysaccharides: implications for second-generation bioethanol production. *BioEnergy Res.* **2013**, *6*, 564−579.
(16) Driemeier, C.; Santos, W. D.; Buckeridge, M. S. Cellulose crystals in fibrovascular bundles of sugarcane culms: orientation, size, distortion, and variability. *Cellulose* **2012**, *19*, 1507−1515.
(17) Sluiter, A.; Ruiz, R.; Scarlata, C.; Sluiter, A.; Templeton, D. *Determination of Extractives in Biomass − Laboratory Analytical Procedure* (LAP; technical report NREL/TP-510-42619); NREL: Golden, CO, Jan 2008.
(18) Moncrieff, D. A.; Robinson, V. N. E.; Harris, L. B. Charge neutralization of insulating surfaces in the SEM by gas ionization. *J. Phys. D−Appl. Phys.* **1978**, *11*, 2315−2325.
(19) Danilatos, G. D. Review and outline of environmental SEM at present. *J. Microsc. Oxford* **1991**, *162*, 391−402.
(20) Donald, A. M. The use of environmental scanning electron microscopy for imaging wet and insulating materials. *Nat. Mater.* **2003**, *2*, 511−516.
(21) Hailwood, A. J.; Horrobin, S. Absorption of water by polymers: analysis in terms of a simple model. *Trans. Faraday Soc.* **1946**, *42*, B084−B092.
(22) Skaar, C. *Wood-Water Relations*; Springer-Verlag: Berlin, Germany, 1988.
(23) Kohler, R.; Alex, R.; Brielmann, R.; Ausperger, B. A new kinectic water sorption isothermas for cellulosic materials. *Macromol. Symp.* **2006**, *244*, 89−96.
(24) Hill, C. A. S.; Keating, B. A.; Jalaludin, Z.; Mahrdt, E. A reological description of the water vapour sorption kinectics behavior of wood invoking a model using a canonical assembly of Kevin-Voigt elements and a possible link with sorption hysteresis. *Holzforschung* **2012**, *66*, 35−47.
(25) Driemeier, C.; Mendes, F. M.; Oliveira, M. M. Dynamic vapor sorption and thermoporometry to probe water in celluloses. *Cellulose* **2012**, *19*, 1051−1063.
(26) Petrov, O. V.; Furó, I. NMR cryoporometry: principles, applications and potential. *Prog. Nucl. Magn. Reson. Spectrosc.* **2009**, *54*, 97−122.
(27) Brun, M.; Lallemand, A.; Quinson, J. F.; Eyraud, C. A new method for the simultaneous determination of the size and the shape of pores: the thermoporometry. *Thermochim. Acta* **1977**, *21*, 59−88.
(28) Driemeier, C.; Bragatto, J. Crystallite width determines monolayer hydration across a wide spectrum of celluloses isolated from plants. *J. Phys. Chem. B* **2013**, *117*, 415−421.
(29) Driemeier, C.; Pimenta, M. T. B.; Rocha, G. J. M.; Oliveira, M. M.; Mello, D. B.; Maziero, P.; Gonçalves, A. R. Evolution of cellulose crystals during prehydrolysis and soda delignification of sugarcane lignocellulose. *Cellulose* **2011**, *18*, 1509−1519.
(30) Ishizawa, C. I.; Davis, M. F.; Schell, D. F.; Johnson, D. K. Porosity and its effect on the digestibility of dilute sulphuric acid pretreated corn stover. *J. Agric. Food Chem.* **2007**, *55*, 2575−2581.
(31) Maloney, T. C.; Paulapuro, H.; Stenius, P. Hydration and swelling of pulp fibers measured with differential scanning calorimetry. *Nord. Pulp Pap. Res. J.* **1998**, *13*, 31−36.
(32) Luukkonen, P.; Maloney, T.; Rantanen, J.; Paulapuro, H.; Yliruusi, J. Microcrystalline cellulose-water interaction − a novel approach using thermoporosimetry. *Pharm. Res.* **2001**, *18*, 1562−1569.
(33) Park, S.; Venditti, R. A.; Jameel, H.; Pawlak, J. J. Changes in pore size distribution during the drying of cellulose fibers as measured by differential scanning calorimetry. *Carbohydr. Polym.* **2006**, *66*, 97−103.
(34) Yu, Z.; Jameel, H.; Chang, H.-M.; Park, S. The effect of delignification of forest biomass on enzymatic hydrolysis. *Bioresour. Technol.* **2011**, *102*, 9083−9089.
(35) Donaldson, L. A. Lignification and lignin topochemistry − an ultrastructural view. *Phytochemistry* **2001**, *57*, 859−873.
(36) Maréchal, Y.; Chanzy, H. The hydrogen bond network in Iβ cellulose as observed by infrared spectrometry. *J. Mol. Struct.* **2000**, *523*, 183−196.
(37) Faix, O. Fourier transform infrared spectroscopy. In *Methods in Lignin Chemistry*; Lin, S. Y., Dence, C. W., Eds.; Springer-Verlag: Berlin, Germany, 1992; pp 83−109.
(38) Rodrigues, B. J.; Faix, O.; Pereira, H. Determination of lignin content of *Eucalyptus Globulus* wood using FTIR spectroscopy. *Holzforschung* **1998**, *52*, 46−50.
(39) Rasul, M. G.; Rudolph, V.; Carsky, M. Physical properties of bagasse. *Fuel* **1999**, *78*, 905−910.
(40) Driemeier, C.; Oliveira, M. M.; Mendes, F. M.; Gómez, E. O. Characterization of sugarcane bagasse powders. *Powder Technol.* **2011**, *214*, 111−116.
(41) Sanjuan, R.; Anzaldo, J.; Vargas, J.; Turrado, J.; Patt, R. Morphological and chemical composition of pitch and fibers from Mexican sugarcane bagasse. *Holz Roh− Werkstoff* **2001**, *59*, 447−450.
(42) Grethlein, H. E. The effect of pore size distribution on the rate of enzymatic hydrolysis of cellulosic substrates. *Nat. Biotechnol.* **1985**, *3*, 155−160.
(43) Arantes, V.; Saddler, J. N. Cellulose accessibility limits the effectiveness of minimum cellulase loading on the efficient hydrolysis of pretreated lignocellulosic substrates. *Biotechnol. Biofuels* **2011**, *4*, 3.
(44) Bragatto, J.; Segato, F.; Cota, J.; Mello, D. B.; Oliveira, M. M.; Buckeridge, M. S.; Squina, F. M.; Driemeier, C. Insights on how the activity of an endoglucanase is affected by physical properties of insoluble celluloses. *J. Phys. Chem. B* **2012**, *116*, 6128−6136.
(45) Leu, S.-Y.; Zhu, J. Y. Substrate-related factors affecting enzymatic saccharification of lignocelluloses: our recent understanding. *BioEnergy Res.* **2012**, DOI: 10.1007/s12155-012-9276-1.